Supporting Information

Experimental Section

Materials: Cobalt(II) nitrate hexahydrate ($Co(NO_3)_2$) and ammonium fluoride (NH_4F) were purchased from Alfa-Aesar and directly used without purification. The carbon cloth was purchased from Japan Toray Company. Sodium nitrate ($NaNO_3$, 99.0%), sodium nitrite ($NaNO_2$, 99.0%), ammonium chloride (NH_4Cl), sodium hydroxide (NaOH), potassium hydroxide (KOH), sodium salicylate ($C_7H_5NaO_3$), trisodium citrate dihydrate ($C_6H_5Na_3O_7 \cdot 2H_2O$), p-dimethylaminobenzaldehyde ($C_9H_{11}NO$), sodium nitroferricyanide dihydrate ($Na_2Fe(CN)_5NO \cdot 2H_2O$), 0.8wt% sulfamic acid solution (H_3NO_3S), sodium dihydrogen phosphate dihydrate (NaH_2PO_4), disodium hydrogen phosphate dodecahydrate (Na_2HPO_4) and sodium hypochlorite solution (NaClO) were purchased from Aladdin Ltd. (Shanghai, China). Ultrapure water used throughout all experiments was purified through a Millipore system.

Characterizations: The crystallinity and composition of the synthesized samples were characterized by X-ray diffraction (XRD; Rigaku Co.) with Cu Kα radiation (λ = 1.5406 Å) and X-ray photoelectron spectroscopy (XPS; ESCALAB250Xi, Thermo Fisher Scientific). The morphological features and detailed structural information were conducted by field-emission scanning electron microscopy (FESEM; GeminiSEM, Zeiss), and transmission electron microscopy (TEM; JEOL JEM-2100F). High-angle annular dark-field scanning transmission electron microscopy (HAADF-STEM) was carried out using a JEOL JEMARM200F STEM/TEM (resolution of 0.08 nm). The absorbance data of spectrophotometer were acquired on SHIMADZU UV-1800 UV-Vis spectrophotometer.

Synthesis of Carbon Paper @ Co_3O_4: A hydrothermal solution was prepared by mixing 2 mmol $Co(NO_3)_2$, 4 mmol NH_4F, 10 mmol urea, and 60 mL of deionized (DI) water. The solution was stirred continuously for 5 minutes and then transferred into Teflon-lined stainless steel autoclave liners. A piece of pressed nickel foam, cleaned with ethanol and DI water, was immersed in the reaction solution. To serve as a current collector, part of the substrate was shielded from contamination using a uniform coating of polytetrafluoroethylene tape. The autoclave was sealed and maintained at 120 ℃ for 6 hours. Afterward, the samples were washed with DI water, dried at 60 ℃ in an oven, and annealed in a furnace under an argon atmosphere at 300 ℃ for 2 hours, resulting in the formation of Co_3O_4.

Synthesis of Carbon Paper @ N-Co_3O_4: The Co_3O_4 obtained above was subjected directly to nitrogen RF plasma treatment at room temperature to synthesize N-Co_3O_4. The plasma discharge was conducted at 200 W power and 13.56 MHz frequency for 20 seconds.

Electrochemical measurements: NO_3^- reduction experiments were carried out in a two-compartment cell under ambient condition, which was separated by Nafion 117 membrane. The membrane was protonated by first boiling in ultrapure water for 1 h and treating in H_2O_2 (5 wt%) aqueous solution at 80 °C for another 1 h, respectively. And then, the membrane was treaded in 0.5 M H_2SO_4 for 3 h at 80 °C and finally in water for 6 h. The electrochemical experiments were carried out with an electrochemical workstation (CHI 660E) using a three-electrode configuration with prepared electrodes, graphite rod and Ag/AgCl electrode (saturated KCl electrolyte) as working electrode, counter electrode and reference electrode, respectively. The

potentials reported in this work were converted to reversible hydrogen electrode (RHE) scale via calibration with the following equation: E (vs. RHE) = E (vs. Ag/AgCl) + 0.059 × pH + 0.197 V and the presented current density was normalized to the geometric surface area. For electrochemical NO_3^- reduction, chrono-amperometry tests were conducted in 1 M KOH solution with 0.1 M NO_3^-.

Determination of NH_3: Owing to the large concentration of solution, the obtained reaction solutions were diluted 100 times. Specifically, 4 mL electrolyte was obtained from the cathodic chamber and mixed with 50 μL oxidizing solution containing NaClO (ρCl = 4 ~ 4.9) and NaOH (0.75 M), 500 μL coloring solution containing 0.4 M $C_7H_6O_3Na$ and 0.32 M NaOH, and 50 μL catalyst solution (1 wt% $Na_2[Fe(CN)_5NO]$) for 2 h. Absorbance measurements were performed at 654 nm. The concentration-absorbance curve was calibrated using standard NH_3 solution with a series of concentrations. The fitting curve ($y = 0.31647\ x + 0.03549$, $R^2 = 0.999$) shows good linear relation of absorbance value with NH_3 concentration.

In addition, ^1H NMR spectroscopy (600 MHz) was also used to detect ammonia in the isotope-labelling measurement. The collected NH_3 sample was first diluted to the detection range and adjust to pH 1.0 by adding 0.1 M HCl. Next, 0.5 ml of the sample solution was mixed 0.1ml DMSO-d_6.

Determination of NO_2^-: Owing to the large concentration of solution, the obtained reaction solutions were diluted 20 times. The NO_2^- concentration was analyzed using the Griess test.[1] The Griess reagent was prepared by dissolving 0.1 g N-(1-naphthyl) ethylenediamine dihydrochloride, 1.0 g sulfonamide and 2.94 mL H_3PO_4 in 50 mL

deionized water. In a typical colorimetric assay, the 1.0 mL Griess reagent was mixed with the 1.0 mL nitrite-containing solution and 2.0 mL H_2O and allowed to react at room temperature for 10 min, in which sulfonamide reacts with NO_2^- to form a diazonium salt and then further reacts with amine to form an azo dye (magenta). The absorbance at 540 nm was measured to quantify the NO_2^- concentration with a standard curve of NO_2^- ($y = 0.5391x + 0.0106$, $R^2 = 0.999$).

Determination of FE and NH_3 yield: The FE for NO_3^- reduction was defined as the amount of electric charge used for synthesizing NH_3 divided the total charge passed through the electrodes during the electrolysis. The total amount of NH_3 produced was measured using colorimetric methods. Assuming eight electrons were needed to produce one NH_3 molecule, the FE could be calculated as follows:

$$FE = 8 \times F \times [NH_3] \times V / (17 \times Q) \times 100\% \quad (1)$$

NH_3 yield was calculated using the following equation:

$$NH_3 \text{ yield rate} = [NH_3] \times V / (s \times t) \quad (2)$$

where F is the Faraday constant, $[NH_3]$ is the measured NH_3 concentration, V is the volume of the electrolyte in the cathodic chamber, Q is the total quantity of applied electricity; t is the reduction time; s is the electrode area.

Computational Details: All the calculations were implemented in the VASP package by employing density functional theory (DFT) with spin-polarized Perdew-Burke-Ernzerhof (PBE) exchange-correlation functional.[1,2] The cutoff energy of plane-wave basis set is 400 eV, and the (2×2×1) grid sampling was used for Brillouin zone integration of Co_3O_4 (110) slab, respectively. The DFT+U method was adopted to

describe the Co 3*d* electrons with an effective U value of 2 eV.[3,4] The convergence criteria of energy and force for structural optimization were set to 1×10^{-5} eV and 0.02 eV/Å, respectively. All the slabs were repeated periodically with a 20 Å vacuum layer between the images in the direction of the surface normal.

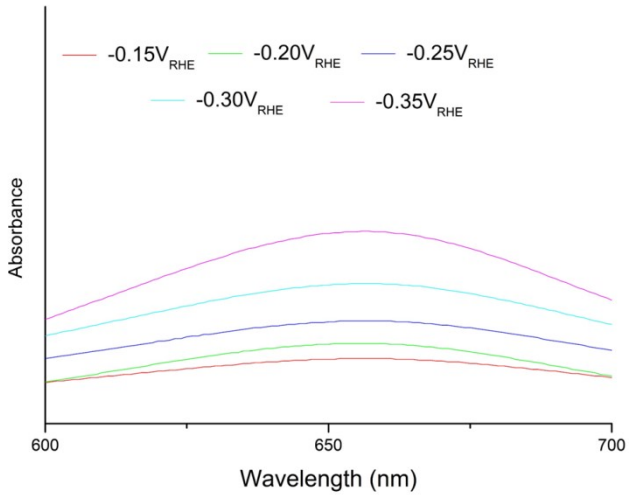

Fig. S1. UV-Vis absorption spectra of N-Co_3O_4.

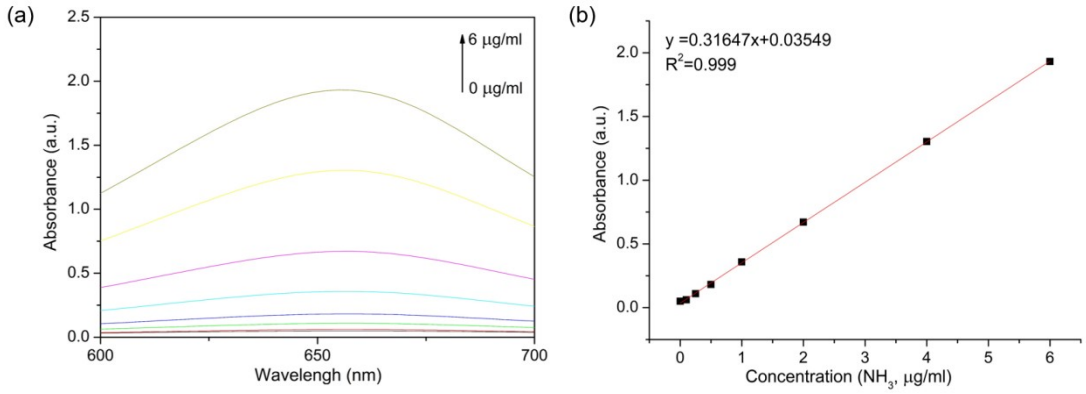

Fig. S2. (a) UV-vis absorption spectra of indophenol assays with NH_3 concentrations after incubated for 2 h at room temperature. (b) Calibration curve used for estimation of NH_3 concentration.

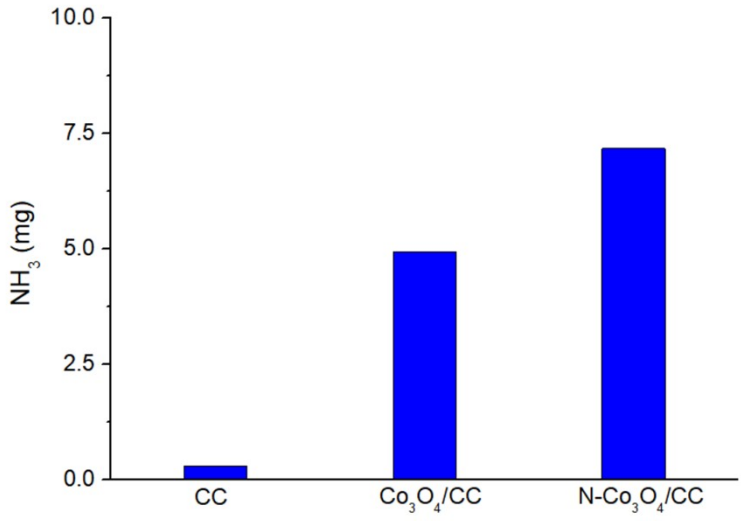

Fig. S3. The comparison of NH_3 production amount on N-Co_3O_4/CC, Co_3O_4/CC and bare CC.

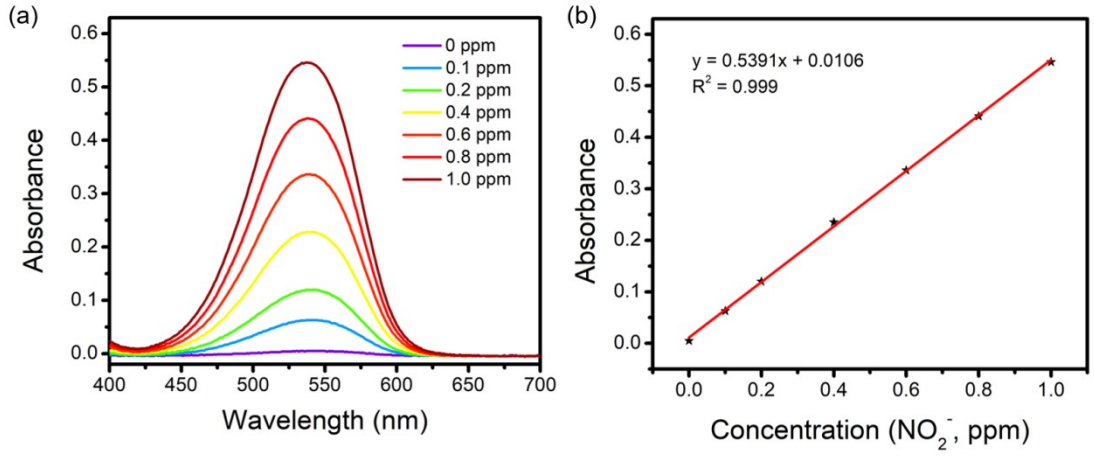

Fig. S4. (a) UV-Vis absorption spectra of different NO_2^- concentrations after incubated for 10 min at room temperature. (b) Calibration curve used for estimation of NO_2^- concentration.

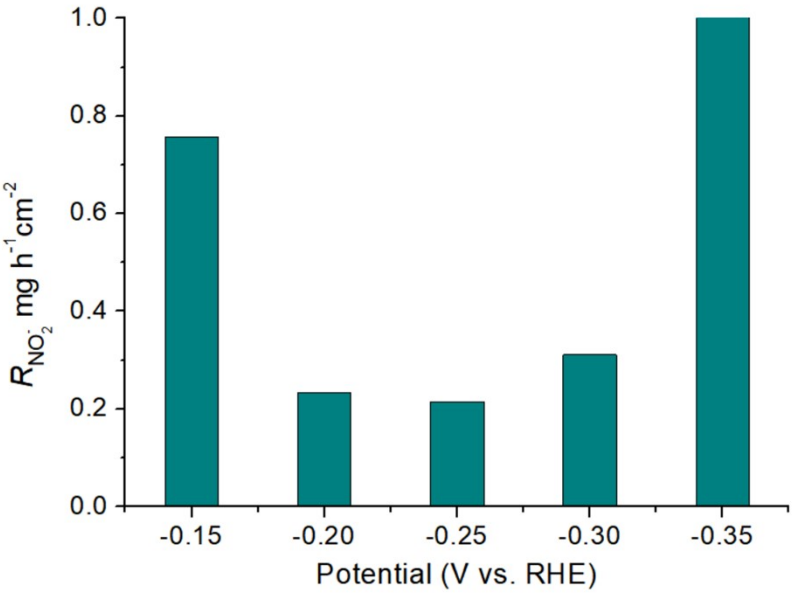

Fig. S5. NO_2^- yield rates over N-Co_3O_4/CC at each given potentials.

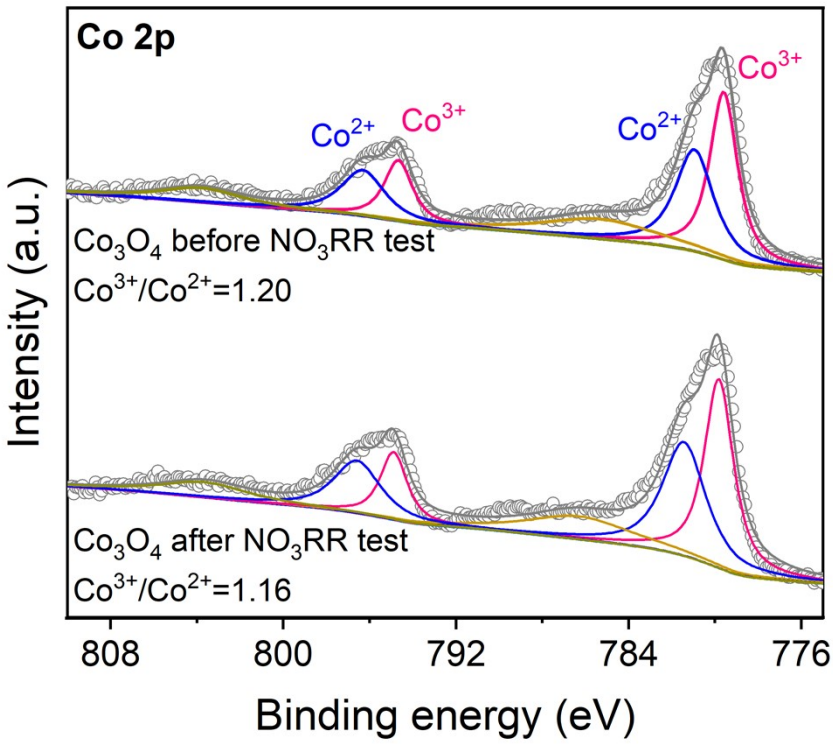

Fig. S6. XPS spectrum in Co 2p region on Co_3O_4/CC after NO_3RR.

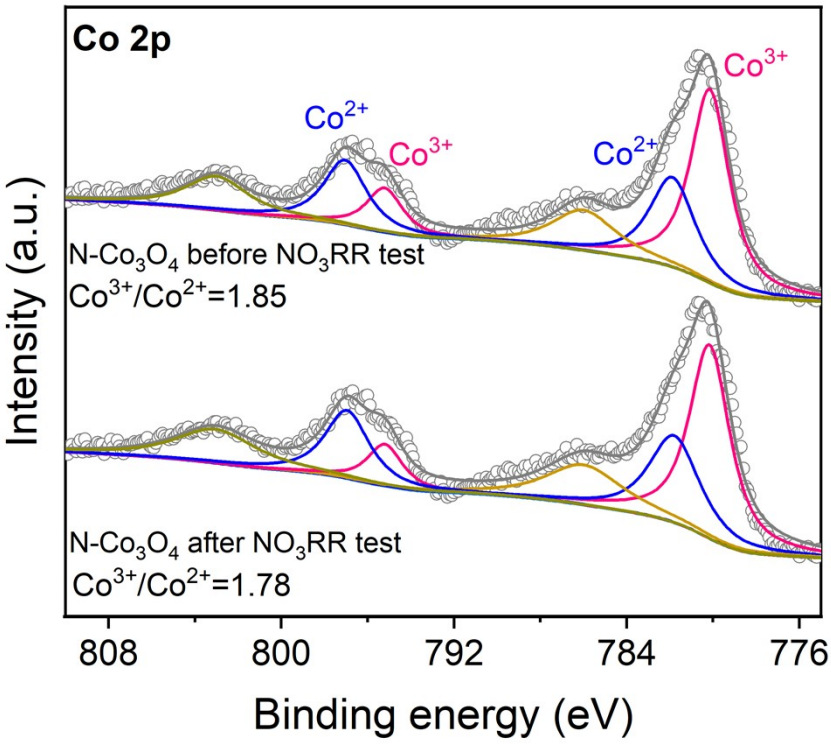

Fig. S7. XPS spectrum in Co 2p region on N-Co_3O_4/CC after NO_3RR.

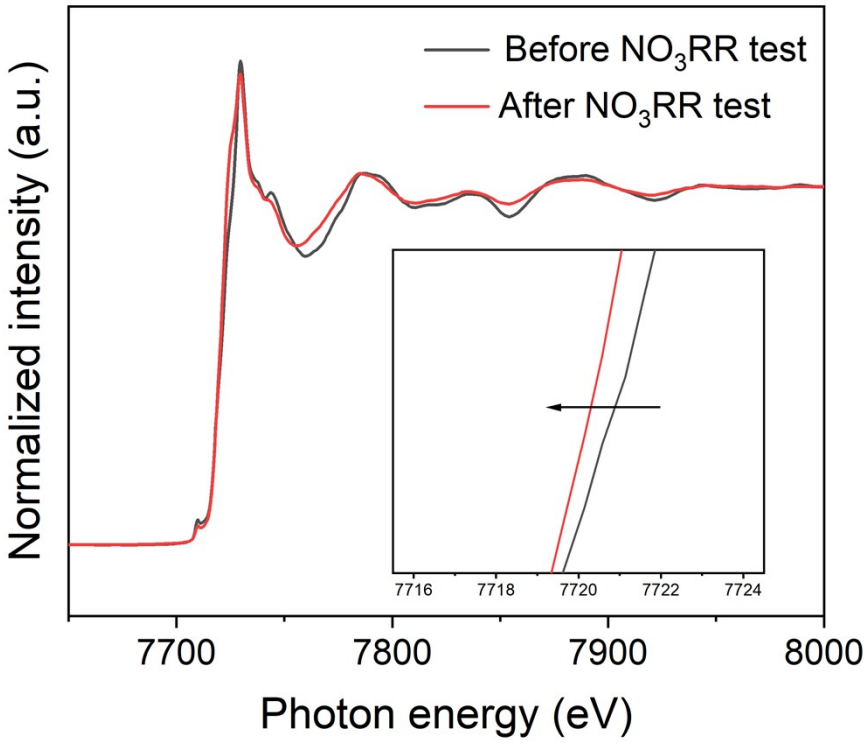

Fig. S8. Co K-edge XANES spectra of N-Co_3O_4 after NO_3RR. It shows that the Co valence state slightly decreases after NO_3RR.

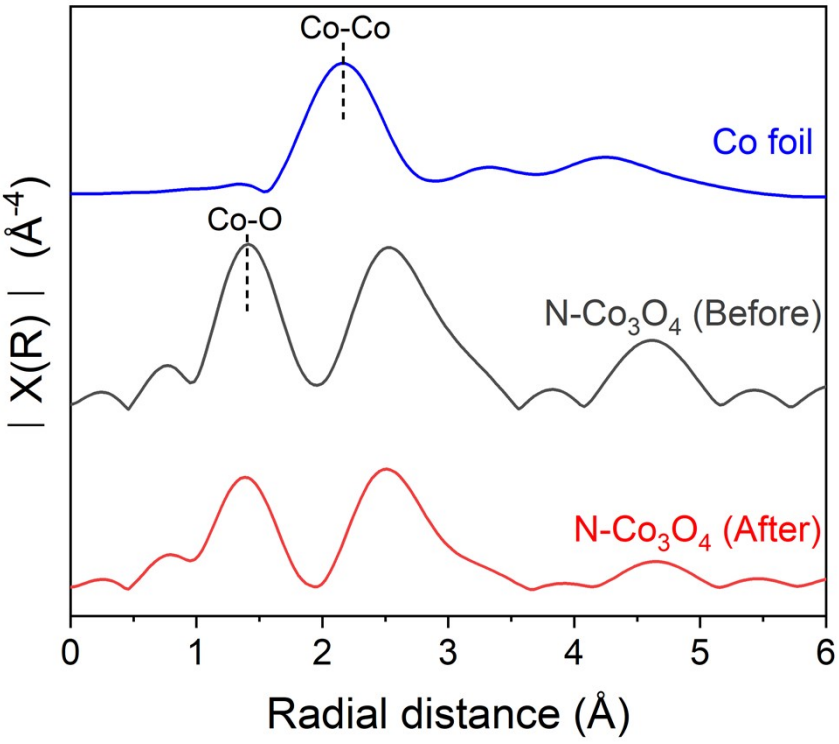

Fig. S9. The Fourier transform EXAFS spectra for N-Co_3O_4 after NO_3RR.

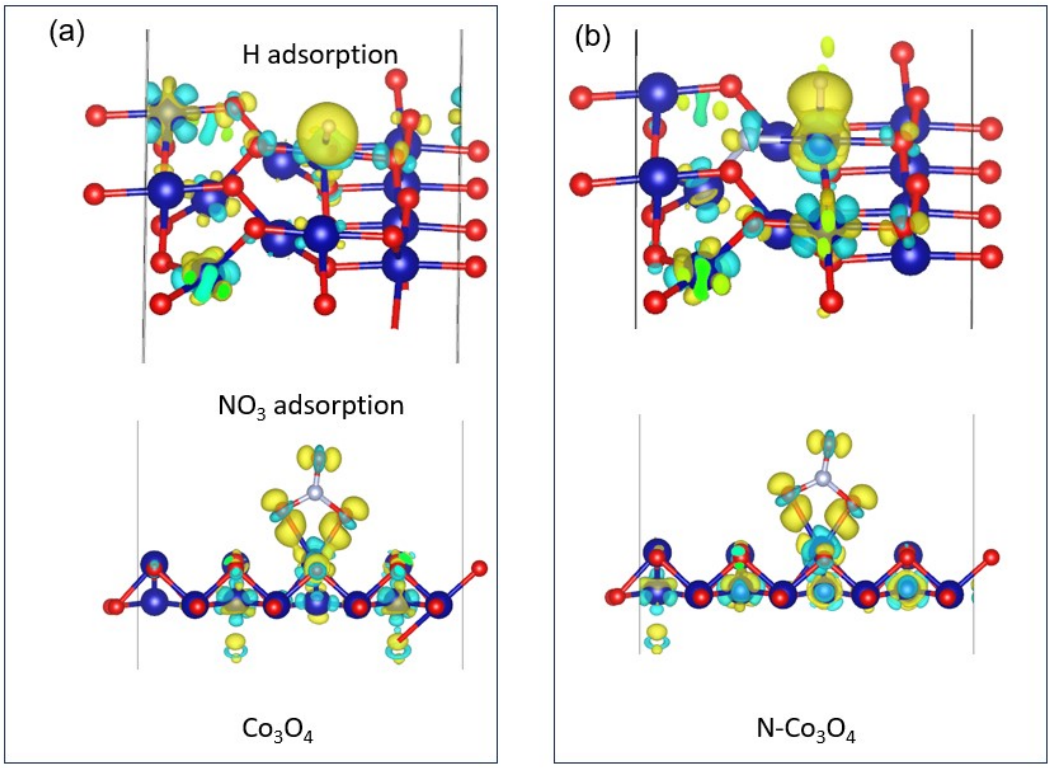

Fig. S10. The atom configurations of NO_3 and H adsorptions on Co_3O_4 (110) and N-Co_3O_4 (110), respectively.

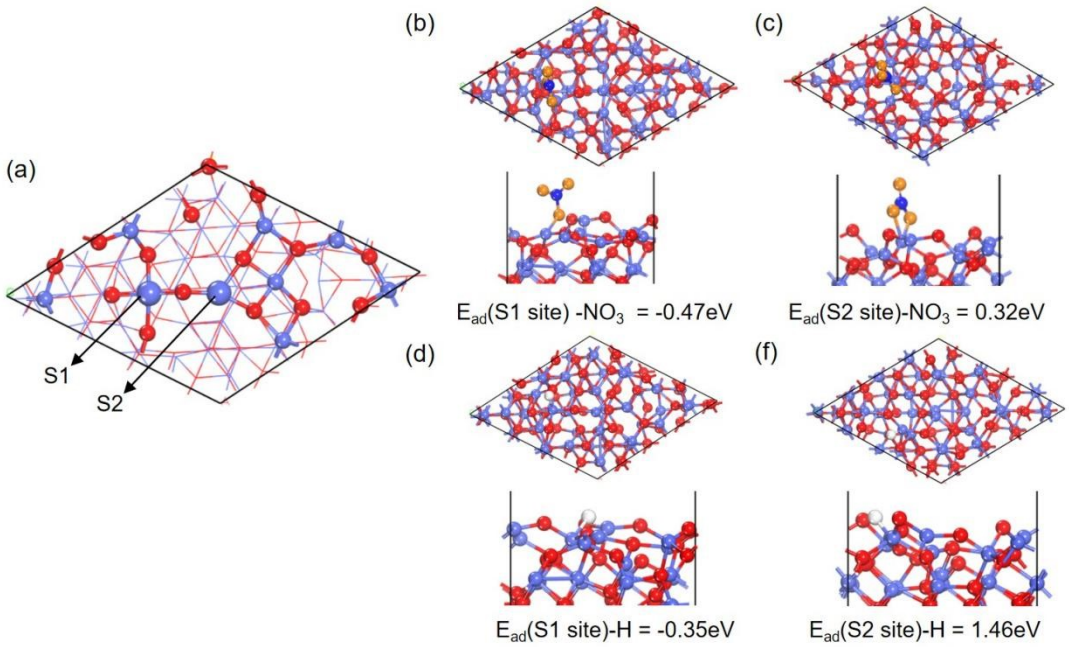

Fig. S11. Adsorption energies of NO_3 and H on Co atom site on pure Co_3O_4 (111) surface. (a) Atomic configuration of Co_3O_4 (111) surface. (a,b) Adsorption energies of NO_3 on Co atom sites. (a,b) Adsorption energies of H on Co atom sites.

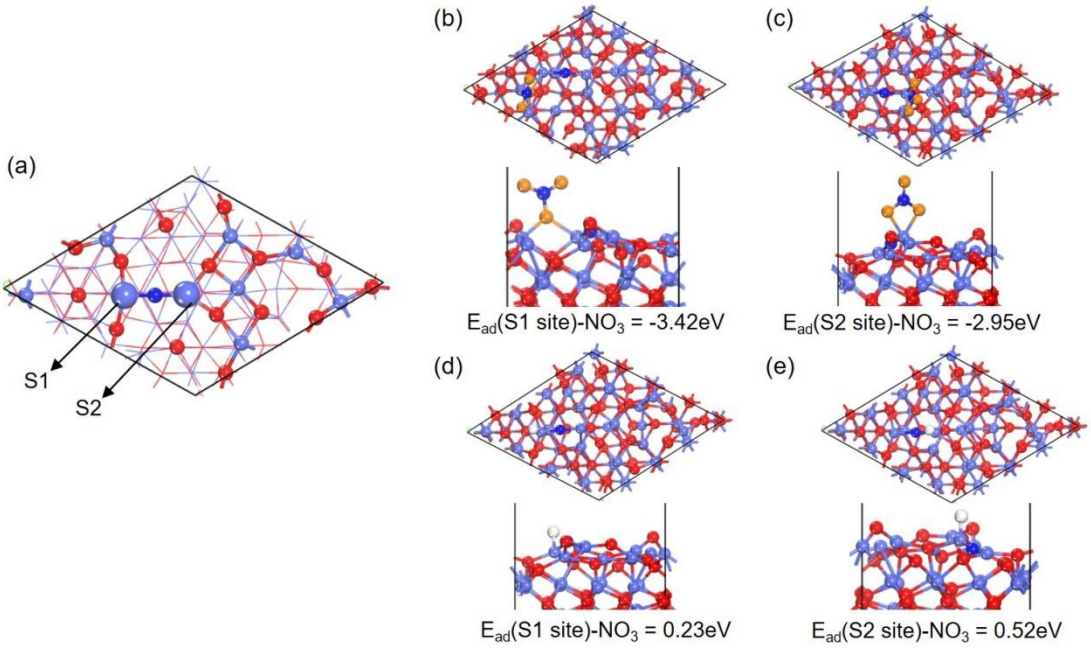

Fig. S12. Adsorption energies of NO_3 and H on Co atom site on N-doped Co_3O_4 (111) surface. (a) Atomic configuration of N-Co_3O_4 (111) surface. (a,b) Adsorption energies of NO_3 on Co atom sites. (a,b) Adsorption energies of H on Co atom sites.

We recalculated the adsorption energies of H and NO_3 on the Co_3O_4 (111) surface, Fig. S11. Our results indicate that the Co_3O_4(111) surface features two distinct Co atomic sites, S1 and S2, corresponding to four-coordinated Co (Co_{4c}) and three-coordinated Co (Co_{3c}), respectively. Both NO_3 and H preferentially adsorb on the Co_{4c} site of S1 due to their exothermic adsorption energies. Notably, the adsorption energies of NO_3 and H at S1 are quite close, with NO_3 being slightly more favorable, suggesting intense competitive adsorption relationship between these species on pure Co_3O_4 (111) surface.

As introducing N doping into the Co_3O_4(111) surface (Fig. S12), the adsorption energies of NO_3 at the S1 and S2 sites are greatly increased to -3.42 eV and -2.95 eV, respectively, indicating greatly enhanced NO_3 adsorption. In contrast, the adsorption of H became endothermic, suggesting that H adsorption process is significantly suppressed. Thus, above results demonstrate that N doping in the Co_3O_4(111) surface also promotes NO_3 adsorption while inhibiting H adsorption, similar with that Co_3O_4(110) surface.

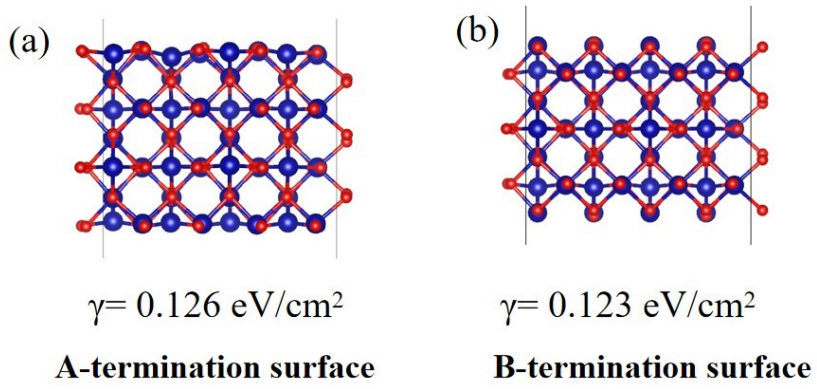

Fig. S13. The surface energies of Co_3O_4 (110) at different terminated conditions. (a) Type A termination surface. (a) Type B termination surface.

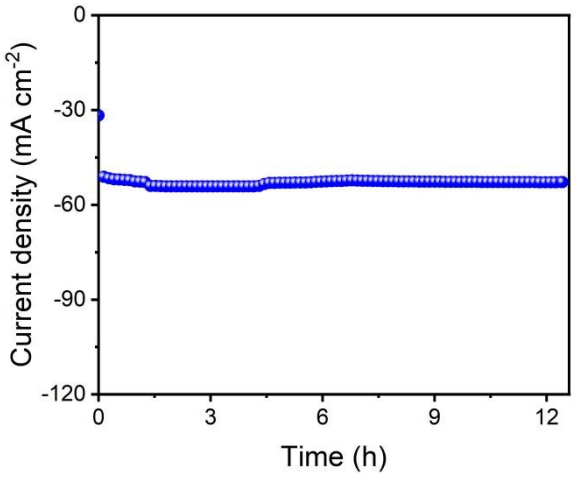

Fig. S14. NO_3RR electrolysis for 13 h on N-Co_3O_4/CC electrode.

Table S1. Comparison of the catalytic performances of CoS_2 OC with reported Co-based NO_3RR catalysts at ambient conditions.

Catalyst	Electrolyte	NH_3 yield rate ($\mu mol\ h^{-1}\ cm^{-2}$@V vs. RHE)	FE (%@V vs. RHE)	Ref.
N-Co_3O_4	1 M KOH (0.1 M NO_3^-)	422@ -0.35V	96.7 %@ -0.20V	This work
CoS_2 OC	1 M KOH (0.1 M NO_3^-)	588 @ -0.35V	97.5 @ -0.25V	[1]
CuCo	1 M KOH (0.1 M NO_3^-)	4800 @ -0.2	100 @ -0.2	[2]
Co@TiO_2/TP	0.1 M PBS (0.1 M NO_3^-)	800 @ -0.40V	96.7 @ -0.70V	[3]
Co-P/TP	0.2 M PBS (200 ppm NO_3^-)	24.47 @ -0.6	93.6 @ -0.3	[4]
Co_2AlO_4/CC	0.1 M PBS (0.1 M NO_3^-)	464.7 @ -0.9	92.6 @ -0.7	[5]
Co/CoO NSA	0.1 M Na_2SO_4 (200 ppm NO_3^-)	194.46 @ -0.65	93.8 @ -0.65	[6]
$ZnCo_2O_4$ NSA/CC	0.1 M NaOH (0.1 M NO_3^-)	634.74 @ -0.8	98.33 @ -0.6	[7]
$CoTiO_{3-x}$/CP	1 M KOH (0.1 M NO_3^-)	858 @ -1.0	92.6 @ -1.0	[8]
$NiCo_2O_4$/CC	0.1 M NaOH (0.1 M NO_3^-)	973.2 @ -0.6	99 @ -0.3	[9]
CoP NAs/CFC	1 M NaOH (1 M NO_3^-)	956 @ -0.3	100 @ -0.3	[10]
Mn-Co_3O_4	0.5 M K_2SO_4 (0.1 M NO_3^-)	2058 @ -1.2	99.5 @ -1.2	[11]
Fe_3C	0.1 M NaOH	466 @ -0.8	96.9 @ -0.8	[12]

NPs@NCF	(0.1 M NO_3^-)			
Cu nanosheets	0.1 M KOH (10 mM KNO_3)	21.67 @ -0.15 V	99.7 @ -0.15 V	[13]
$FeCo_2O_4$	0.1 M NaOH (20 mM $NaNO_3$)	277.1 @ -0.5V	95.9	[14]
$Cu_{50}Ni_{50}$	1 M KOH (100 mM NO_3^-)	80.7 @ -0.15	82.0 @ -0.15	[15]
Fe_3O_4/PC	0.1 M NaOH (0.1 M NO_3^-)	394.8 @ -0.4	91.6 @ -0.4	[16]

REFERENCES

[1] W. Li, P. Wang, P. Wang, H. Liu, C. Wu, Y. Liu, J. Huang, Z. Fang, H. Guo, Y. Zhang, F. Li, T. Wu and X. Sun, Octahedral CoS_2 electrocatalysts for efficient nitrate reduction to ammonia, *Inorg. Chem. Front.*, 2024, **11**, 7118.

[2] J. Fang, Q. Zheng, Y. Lou, K. Zhao, S. Hu, G. Li, O. Akdim, X. Huang and S. Sun, Ampere-level current density ammonia electrochemical synthesis using CuCo nanosheets simulating nitrite reductase bifunctional nature, *Nat. Commun.,* 2022, **13**, 7899.

[3] X. Fan, D. Zhao, Z. Deng, L. Zhang, J. Li, Z. Li, S. Sun, Y. Luo, D. Zheng, Y. Wang, B. Ying, J. Zhang, A. A. Alshehri, Y. Lin, C. Tang, X. Sun and Y. Zheng, Constructing Co@TiO_2 nanoarray heterostructure with schottky contact for selective electrocatalytic nitrate reduction to ammonia, *Small,* 2023, **19**, 2208036.

[4] Z. Li, G. Wen, J. Liang, T. Li, Y. Luo, Q. Kong, X. Shi, A. M. Asiri, Q. Liu and X. Sun, High-efficiency nitrate electroreduction to ammonia on electrodeposited cobalt‐phosphorus alloy film, *Chem. Commun.,* 2021, **57**, 9720.

[5] Z. Deng, J. Liang, Q. Liu, C. Ma, L. Xie, L. Yue, Y. Ren, T. Li, Y. Luo, N. Li, B. Tang, A. A. Alshehri, I. Shakir, P. O. Agboola, S. Yan, B. Zheng, J. Du, Q. Kong and X. Sun, High-efficiency ammonia electrosynthesis on self-supported

Co_2AlO_4 nanoarray in neutral media by selective reduction of nitrate, *Chem. Eng. J.,* 2020, **435**, 135104.

[6] Y. Yu, C. Wang, Y. Yu, Y. Wang and B. Zhang, Promoting selective electroreduction of nitrates to ammonia over electron-deficient Co modulated by rectifying Schottky contacts, *Sci. China Chem.,* 2020, **63**, 1469.

[7] Z. Li, J. Liang, Q. Liu, L. Xie, L. Zhang, Y. Ren, L. Yue, N. Li, B. Tang, A. A. Alshehri, M. S. Hamdy, Y. Luo, Q. Kong and X. Sun, High-efficiency ammonia electrosynthesis via selective reduction of nitrate on $ZnCo_2O_4$ nanosheet array, *Mater. Today Phy.,* 2022, **23**, 100619.

[8] X. Fan, J. Liang, L. Zhang, D. Zhao, L. Yue, Y. Luo, Q. Liu, L. Xie, N. Li, B. Tang, Q. Kong and X. Sun, Enhanced electrocatalytic nitrate reduction to ammonia using plasma-induced oxygen vacancies in $CoTiO_{3-x}$ nanofiber, *Carbon Neutralization,* 2022, **1**, 6.

[9] Q. Liu, L. Xie, J. Liang, Y. Ren, Y. Wang, L. Zhang, L. Yue, T. Li, Y. Luo, N. Li, B. Tang, Y. Liu, S. Gao, A. A. Alshehri, I. Shakir, P. O. Agboola, Q. Kong, Q. Wang, D. Ma and X. Sun, Ambient Ammonia Synthesis via Electrochemical Reduction of Nitrate Enabled by $NiCo_2O_4$ Nanowire Array, *Small,* 2022, **18**, 2106961.

[10] S. Ye, Z. Chen, G. Zhang, W. Chen, C. Peng, X. Yang, L. Zheng, Y. Li, X. Ren, H. Cao, D. Xue, J. Qiu, Q. Zhang and J. Liu, Elucidating the activity, mechanism and application of selective electrosynthesis of ammonia from nitrate on cobalt phosphide, *Energy Environ. Sci.,* 2022, **15**, 760.

[11] D. Liu, L. Qiao, Y. Chen, P. Zhou, J. Feng, C. C. Leong, K. W. Ng, S. Peng, S. Wang, W. F. Ip and H. Pan, Electrocatalytic reduction of nitrate to ammonia on low-cost manganese-incorporated Co_3O_4 nanotubes, *Appl. Catal., B,* 2023, **324**, 122293.

[12] X. Liu, T. Xie, Z. Cai, Z. Li, L. Zhang, X. Fan, D. Zhao, S. Sun, Y. Luo, Q. Liu, and X. Sun, Fe_3C nanoparticles decorated 3D nitrogen-doped carbon foam as a highly efficient electrocatalyst for nitrate reduction to ammonia. *J. Electroanal. Chem.*, 2023, **933**, 117295.

[13] X. Fu, X. Zhao, X. Hu, K. He, Y. Yu, T. Li, Q. Tu, X. Qian, Q. Yue, M. R. Wasielewski, Y. Kang, Alternative route for electrochemical ammonia synthesis by reduction of nitrate on copper nanosheets. *Appl. Mater. Today*, 2020, ***19***, 100620.

[14] J. Li, D. Zhao, L. Zhang, L. Yue, Y. Luo, Q. Liu, N. Li, A. A. Alshehri, M. S. Hamdy, Q. Li, X. Sun, A $FeCo_2O_4$ nanowire array enabled electrochemical nitrate conversion to ammonia. *Chem. Commun.*, **2022**, 58, 4480-4483.

[15] Y. Wang, A. Xu, Z. Wang, L. Huang, J. Li, F. Li, J. Wicks, M. Luo, D. Nam, C. Tan, Y. Ding, J. Wu, Y. Lum, C. Dinh, D. Sinton, G. Zheng and E. Sargent, Enhanced nitrate-to-ammonia activity on copper-nickel alloys via tuning of intermediate adsorption. J. Am. Chem. Soc., 2020, 142, 5702-5708.

[16] T. Xie, Z. Cai, X. Liu, J. Li, X. Fan, X. He, Y. Luo, D. Zheng, S, Sun, S. Alfaifi, C. Xu, X. Sun, Fe_3O_4 nanoparticle-decorated 3D pinewood-derived carbon for high-efficiency electrochemical nitrate reduction to ammonia. *Chem. Commun.*, 2023, 59, 12322-12325.